

Peristaltic Transport of Non-Newtonian Fluid under Effects of Magnetic Force and Heat Transfer in a Symmetric Channel through a Porous Medium

Amaal Mohi Nassief*  , Ahmed M. Abdulhadi  

Department of Mathematics, College of Science, University of Baghdad, Baghdad, Iraq.

*Corresponding Author.

Received 25/09/2022, Revised 24/03/2023, Accepted 26/03/2023, Published Online First 20/09/2023, Published 01/04/2024



© 2022 The Author(s). Published by College of Science for Women, University of Baghdad.

This is an Open Access article distributed under the terms of the [Creative Commons Attribution 4.0 International License](https://creativecommons.org/licenses/by/4.0/), which permits unrestricted use, distribution, and reproduction in any medium, provided the original work is properly cited.

Abstract

In this paper, the effect of magnetic force and nonlinear thermal radiation for peristaltic transport of hybrid bio-nanofluid with the porous medium in a symmetric channel is discussed. The Adomain decomposition technique is utilized for explaining expressions for axial velocity, stream function, temperature, Nusselt number, pressure gradient, magnetic pressure, and magnetic force. The finding shows that gold nanoparticles have an elevation velocity compared with copper nanoparticles, based fluids, and hybrid nanofluids. The magnetic force contours increase when the wave amplitude increases. The temperature and heat transfer rate have been examined clearly. It has been observed that rising thermal radiation increases temperatures. Lastly, the phenomenon of trapping is presented to explain the physical behavior of different parameters. The effects of physical parameters are examined through graphs by using the MATHEMATICA software

Keywords: Magnetic force, Peristaltic transport, Porous medium, Symmetric channel, Thermal radiation.

Introduction

Non-Newtonian fluids have received a lot of interest in relation to peristalsis due to their diverse applications in industrial and physiologic processes. Peristaltic transport is a simple form of fluid flow generated by a progressive wave of area reduction or expansion over the length of an elongated tube containing fluid. It is a fundamental characteristic of most biological systems that they contain smooth muscular tubes that carry biological fluids during propulsive movement. It is present in a variety of glandular ducts, including those that transport urine from the kidney to the bladder and chime movement in the gastrointestinal tract. Blood

flow is non-Newtonian fluid and is a good example of peristaltic flow. The peristaltic transport technique has been used during surgical operations such as blood pumps in heart-lung machines. Despite the fact that peristalsis is well known in physiology, it was only recently discovered to be relevant Latham¹ was a pioneer in this field, Shapiro et al² researchers have created a wide variety of functional nanoparticles during the past few decades. For instance, copper nanoparticles, gold nanoparticles, and magnetic nanoparticles. Gold and copper are utilized as delivery vehicles for drugs in cancer patients. Because of gold particles

are so small, they can pierce the entire body or accumulate in tumor areas due to their physical and chemical properties, their ability to absorb heat, and their increased permeability^{3,4}. Copper is a major component that is required as a cofactor for the effective operation of a variety of metabolic enzymes. It also has antibacterial, antifungal, and anti-inflammatory properties. That makes it useful for making microbial resistant, ointments and bandages⁵. Much research has been published on the peristaltic analyze. Zhang et al.⁶ discussed an entropy study of blood flow propagating through an anisotropically tapered artery under the suspension of magnetic Zane-oxide nanoparticles. The peristaltic of couple stress nanofluid organized by the presence of electrical field and magnetic field into micro channel were discussed by Tripathi et al⁷. Mishra et al.⁸ solved a problem on heat transfer and entropy generation in blood flow while holding gold nanoparticles in an asymmetrical channel with electro osmotic processes. Hussain et al.⁹ examined thermal analysis under the influence of magnetic and gravitational forces through a uniformly inclined channel using Casson fluid as the base fluid and tiny gold particles. Noreen et al¹⁰ studied the effect of copper particles on the motion of blood in a vertical channel in the being of heat convection. Rashid et al.¹¹ discussed the Williamson fluid with

Materials and Methods

Mathematical Formulation:

The unsteady flow of hydro-magnetic, viscous, electrically conducting, and incompressible hybrid bio-nanofluid (blood and Cu-Au nanoparticles) is considered in a two-dimensional symmetric channel. Also, it is the propagation of sinusoidal waves down towards the channel's wall through a porous medium with a uniform cross section. The rectangular coordinate system X, Y is specified with X -axis aligned with the channel's centerline and Y -axis aligned with the channel's transverse direction. the external magnetic field of strength H_0 is applied to the system, resulting in an induced magnetic field $H(H_x(x, y, t), H_y(x, y, t), 0)$, therefore the total magnetic field becomes $H^*(H_x(x, y, t), H_y(x, y, t) + H_0, 0)$. The plate of channel walls is considered to be nonconductive and Fig 1 show the geometry of 2-

induced magnetic field effects. Abo-Elkhair. et al¹² examined the thermal radiation and magnetic force on bio-nanofluid via a peristaltic channel with a moderate Reynolds number, but they did not use a porous medium in their study. Murad and Abdulhadi¹³ investigated the effects of heat transfer and mass transfer on peristaltic flow of Bingham plastic fluid via symmetric channels using porous medium in the existence of a magnetic field. In addition, many researchers were interested in magneto hydrodynamic and heat to peristaltic flow since it was investigated by Khudair and Dwail¹⁴, Al-Khafajy¹⁵, Kareem and Abdulhadi¹⁶, Ahmed et al¹⁷, Musawi and Abdulhadi¹⁸, Jawad and Abdulhadi¹⁹.

Concerning our contribution in this paper, we used a proposed mathematical model to examine the magnetic force and thermal radiation effects on peristaltic transport of hybrid bio-nanofluids in the presence of a magnetic field through a symmetric channel with a porous medium. Gold and copper are considered here as nanoparticles, while blood is considered to be a non-Newtonian base fluid. The precise expressions for axial velocity, stream function, temperature, pressure gradient, Nusselt number, and magnetic force are obtained. Graphs are utilized to explain the impact of physical parameters on flow.

D peristaltic transport with a defined equation for a wall surface:

$$\bar{\xi}(\bar{X}, \bar{t}) = d_0 - d_1 \cos\left[\frac{2\pi}{\lambda}(\bar{X} - c\bar{t})\right], \quad 1$$

where d_0 is the half channel width, d_1 denotes the wave amplitude, and the wavelength is λ , where c is wave speed, X is the direction of the wave propagation and t is the time.

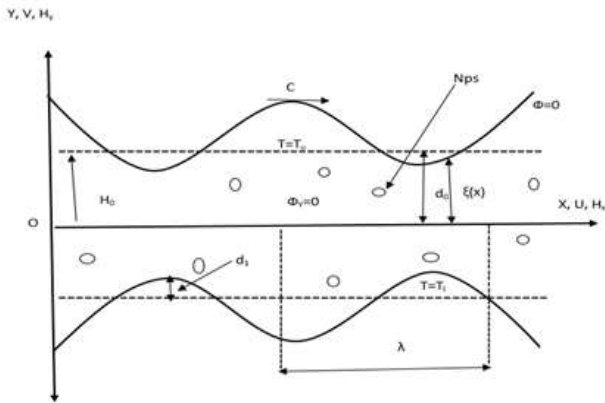


Figure 1. Geometry of problem

The governing equations for the problem:

$$\nabla \cdot \mathbf{E} = 0, \nabla \cdot \mathbf{H} = 0, \mathbf{J} = \nabla \times \mathbf{H}, \sigma[\mathbf{E} + \mu_e(\mathbf{V} \times \mathbf{H})] = \mathbf{J},$$

$$\nabla \times \mathbf{E} = -\mu_e \frac{\partial \mathbf{H}}{\partial t}, \quad 2$$

Where \mathbf{J} is current density, σ is electrical conductivity, \mathbf{E} is electric field, \mathbf{V} is velocity vector and μ_e is magnetic permeability. The governing momentum, heat equations and induction equation of unsteady of viscous incompressible hybrid bio-nanofluid are²⁰

$$\nabla \cdot \mathbf{V} = 0 \quad 3$$

$$\rho_{nf} \frac{D\mathbf{V}}{Dt} = -\nabla P + \mu_{nf} \nabla^2 \mathbf{V} + \mu_e (\mathbf{H}^* \cdot \nabla) \cdot \mathbf{H}^* - \mu_e \frac{\nabla H^{*2}}{2} - \frac{\mu_{nf}}{\eta} \mathbf{V}, \quad 4$$

$$\frac{\partial \mathbf{H}^*}{\partial t} = \nabla \times (\mathbf{V} \times \mathbf{H}^*) + \frac{1}{\zeta} \nabla^2 \mathbf{H}^*, \quad 5$$

$$(\rho c_p)_{nf} \frac{DT}{Dt} = k_{nf} \nabla^2 T + \mu_{nf} (\nabla \mathbf{V} + (\nabla \mathbf{V})^T)^2 - \frac{\partial q}{\partial Y} + Q_0, \quad 6$$

where $\frac{D}{Dt}$ is the total derivative, P is fluid pressure, $\zeta = \mu_e \sigma_{nf}$ is the magnetic diffusivity, σ_{nf} is the electrical conductivity, T is

the temperature distribution, $q = -\frac{4\sigma_f^* \partial T^4}{3k_f^* \partial Y}$ is the radiative heat flux, k_f^* and σ_f^* are mean absorption coefficient and Stefan Boltzmann constants respectively, Q_0 is the heat source, experimental formulation for the physical characteristics of hybrid nanofluid are show in Table 1, which are given by²⁰

Table 1. physical properties of hybrid nanofluid

Property	Nanofluids
Density	$\rho_{nf} = ((1 - \phi_1)\rho_f + \phi_1\rho_1)(1 - \phi_2) + \phi_2\rho_2$
Heat capacity	$(\rho c_p)_{nf} = ((\rho c_p)_f(1 - \phi_1) + (\rho c_p)_1\phi_1)(1 - \phi_2) + (\rho c_p)_2\phi_2$
Dynamic viscosity	$\mu_{nf} = \frac{\mu_f}{(1 - \phi_2)^{2.5}(1 - \phi_1)^{2.5}}$
Thermal conductivity	$k_{nf} = \left(\frac{k_2 + (m - 1)k_3 - (k_3 - k_2)\phi_2(m - 1)}{k_3(m - 1) + k_2 + \phi_2(k_3 - k_2)} \right) k_3$ $= \left(\frac{k_1 + k_f(m - 1) - (k_f - k_1)(m - 1)}{k_1 + \phi_1(k_f - k_1) + k_f(m - 1)} \right) k_3$
Electrical conductivity	$\sigma_{nf} = \sigma_3 \left(\frac{\sigma_2(1 + 2\phi_2) + 2(1 - \phi_2)\sigma_3}{\sigma_3(2 + \phi_2) + \sigma_2(1 - \phi_2)} \right)$ $\sigma_3 = \sigma_f \left(\frac{\sigma_1(1 + 2\phi_1) + 2\sigma_f(1 - \phi_1)}{\sigma_1(1 - \phi_1) + \sigma_f(2 + \phi_1)} \right)$

where ϕ_1 and ϕ_2 are the volume fraction of gold and copper nanoparticles, m represents the shape factor of the proposed nanoparticles, the physical characteristics of nanoparticles are classified in Table 2²¹

Table 2. Based fluid and nanoparticles properties

Properties	Based fluid	Nanoparticle (Gold Au)	Nanoparticle (Copper Cu)
ρ density	$\rho_f = 1050$	$\rho_1 = 19300$	$\rho_2 = 8933$
C_p heat capacity	$C_{pf} = 3617$	$C_{p1} = 129$	$C_{p2} = 385$
K thermal conductivity	$k_f = 0.52$	$k_1 = 318$	$k_2 = 401$
σ electrical conductivity	$\sigma_f = 1.33$	$\sigma_1 = 4.1 * (10^7)$	$\sigma_2 = 5.96 * (10^7)$

For unsteady 2-D flows $\vec{V} = [\bar{U}(\bar{X}, \bar{Y}, \bar{t}), \bar{V}(\bar{X}, \bar{Y}, \bar{t}), 0]$, where \bar{U} is velocity component in coordinate \bar{X} and \bar{V} is the velocity component in coordinate \bar{Y} .

The following transformations are used to convert all equations in our study from fixed to movable frame (\bar{x}, \bar{y}) define as

$$\left. \begin{aligned} x &= \frac{\bar{x}}{\lambda}, y = \frac{\bar{y}}{d_0}, u = \frac{\bar{u}}{c}, v = \frac{\bar{v}}{c}, p = \frac{d_0^2 \bar{p}}{c \lambda \mu_f}, \delta = \frac{d_0}{\lambda}, H_x = \frac{\bar{H}_x}{H_0}, H_y = \frac{\bar{H}_y}{H_0}, \eta = \frac{\bar{\eta}}{d_0^2} \\ \theta &= \frac{T - T_u}{T_l - T_u}, Re = \frac{\rho_f c d_0}{\mu_f}, R_m = \sigma_f \mu_e c d_0, S^2 = \frac{M^2}{Re R_m}, M = H_0 d_0 \sqrt{\frac{\sigma_f}{\mu_f}}, Pr = \frac{\mu_f (c_p)_f}{k_f} \\ E_c &= \frac{c^2}{(c_p)_f (T_l - T_u)}, R_d = \frac{4 \sigma_f^* (T_l - T_u)^3}{3 k_f^* k_f}, \beta = \frac{Q_0 d_0^2}{k_f (T_l - T_u)}, \phi = \frac{\bar{\phi}}{H_0 d_0}, E = -\frac{\bar{E}}{c H_0 \mu_e} \\ A_1 &= \frac{\rho_{nf}}{\rho_f}, A_2 = \frac{\mu_{nf}}{\mu_f}, A_3 = \frac{\sigma_{nf}}{\sigma_f}, A_4 = \frac{k_{nf}}{k_f}, A_5 = \frac{(\rho c_p)_{nf}}{(\rho c_p)_f}, \epsilon = \frac{d_1}{d_0} \end{aligned} \right\} \quad 10$$

In the above expressions, T_u is temperature at upper wall, T_l is temperature at lower wall, $\bar{\psi}$ is stream function, $\bar{\phi}$ is magnetic force function, E is electric field strength, δ is wavenumber, η is permeability parameter, Re is the Reynolds number, E_c is Eckert number, Pr is Prandtl number, M is Hartmann number, R_m is the magnetic Reynolds number, β is the internal heat generations, θ is the temperature in the non-dimensional form, and S is the magnetic force number (Stommer's number).

And we define dimensionless magnetic force function ϕ and stream function ψ through

$$u = \psi_y, v = -\delta \psi_x, H_x = \phi_y, H_y = -\delta \phi_x$$

by using transformation and introducing the dimensionless quantities into Eq. 3 to Eq. 6, the flow equations in terms of stream function ψ and magnetic force ϕ are

$$\begin{aligned} A_1 Re \delta (\psi_y \psi_{xy} - \psi_x \psi_{yy}) &= -(P_m)_x + \\ A_2 \nabla^2 \psi_y + S^2 Re (\delta \phi_y \phi_{xy} - \delta \phi_x \phi_{yy} + \phi_{yy}) &- \\ \frac{A_2}{\eta} (\psi_y + 1), & \quad 11 \end{aligned}$$

$$\begin{aligned} A_1 Re \delta^3 (\psi_y \psi_{xx} - \psi_x \psi_{yy}) &= (P_m)_y + \\ A_2 \delta^2 \nabla^2 \psi_x + S^2 Re \delta^2 (\delta \phi_y \phi_{xx} - \delta \phi_x \phi_{xy} + \phi_{xy}) &+ \\ \frac{A_2}{\eta} \delta^2 \psi_x, & \quad 12 \end{aligned}$$

$$E = (\psi_y - \delta (\psi_y \phi_x - \psi_x \phi_y)) + \frac{1}{A_3 R_m} \nabla^2 \phi, \quad 13$$

$$\bar{X} = \bar{x} + c\bar{t}, \bar{Y} = \bar{y}, \bar{U} = \bar{u} + c, \bar{V} = \bar{v}, \quad 9$$

where \bar{u}, \bar{v} are the velocity components, presenting the dimensionless quantities which are used to find the non-dimensional analysis as

$$\begin{aligned} A_5 Re Pr \delta (\psi_y \theta_x - \psi_x \theta_y) &= A_4 \nabla^2 \theta + \\ A_2 E_c Pr (4 \delta^2 \psi_{xy}^2 + (\psi_{yy} - \delta^2 \psi_{xx})^2) &+ \\ R_d (\theta^4)_{yy} + \beta, & \quad 14 \end{aligned}$$

By using cross derivation to eliminate the pressure between Eq.11 and Eq.12 the next result is obtained:

$$\begin{aligned} A_1 Re \delta (\psi_y \nabla^2 \psi_x - \psi_x \nabla^2 \psi_y) &= A_2 \nabla^4 \psi + \\ S^2 Re (\delta \phi_y \nabla^2 \phi_x - \delta \phi_x \nabla^2 \phi_y + \nabla^2 \phi_y) &- \frac{A_2}{\eta} \nabla^2 \psi, \\ 15 \end{aligned}$$

For the wall dimensional stream, temperature functions and magnetic force in the wave frame, the boundary conditions for non-conductive elastic walls are:

$$\begin{aligned} \psi &= 0, \phi_y = 0, \psi_{yy} = 0, \quad \text{at } y = 0, \\ \phi &= 0, \psi_y = -1, \theta = 0, \psi = \frac{q}{2}, \quad \text{at } y = \xi[x] \\ \theta &= 1 \quad \text{at } y = -\xi[x], \quad 16 \end{aligned}$$

Where q is the mean flow rate and the peristaltic wall's non-dimensional surface is:

$$\xi[x] = 1 - \epsilon \cos[2\pi x]$$

Adomian Decomposition Method:

This method can be utilized to solve linear and non-linear differential equations as well as integral equations, and it produces better results than homotopy perturbation method^{22,23}. George Adomian first proposed this method, and considerable work has been done to solve a variety

of problems²⁴⁻²⁶. The unknown functions $\psi(x, y)$, $\theta(x, y)$ and $\phi(x, y)$ to the formulated equations into the sum of infinite numbers defined by the following decomposition series:

$$\begin{aligned} \psi(x, y) &= \sum_{m=0}^{\infty} \psi_m(x, y), \quad \theta(x, y) \\ &= \sum_{m=0}^{\infty} \theta_m(x, y), \quad \phi(x, y) \\ &= \sum_{m=0}^{\infty} \phi_m(x, y), \end{aligned} \quad 17$$

the decomposition method related itself with finding the components $(\psi_0, \psi_1, \dots, \psi_m)$, $(\theta_0, \theta_1, \dots, \theta_m)$ and $(\phi_0, \phi_1, \dots, \phi_m)$, ($m \geq 0$), individually. These components can be got readily obtaining a relationship contain simple integrals, in the present problem, we solve $L_2(\psi)$, $L_1(\theta)$ and $L_1(\phi)$. As a result, the other linear operators, simply $R1$, $R2$, and $R3$ operators in the system of partial differential equations as follows:

$$\begin{aligned} L_2\psi + R1 + N_1 &= G_1(x, y), L_1\phi + R2 + N_2 = \\ G_2(x, y), L_1\theta + R3 + N_3 &= G_3(x, y), \end{aligned} \quad 18$$

where N_1, N_2 and N_3 are the nonlinear terms, $L_1 = \frac{\partial^2}{\partial y^2} (*)$ (the second order differential operators), and $L_2 = \frac{\partial^4}{\partial y^4} (*)$ (the fourth order differential operators), therefore

$$\begin{aligned} L_2\psi &= G_1(x, y) - R1 - N_1, L_1\phi = G_2(x, y) - \\ R2 - N_2, L_1\theta &= G_3(x, y) - R3 - N_3, \end{aligned} \quad 19$$

On both sides, the inverse operation,

$$L_1^{-1} (*) = \int_0^y \int_0^y (*) dy dy \text{ and}$$

$$L_2^{-1} (*) = \int_0^y \int_0^y \int_0^y \int_0^y (*) dy dy dy dy, \text{ yields}$$

$$\begin{aligned} L_2^{-1}(L_2\psi) &= L_2^{-1}(G_1(x, y) - R1 - \\ N_1), L_1^{-1}(L_1\phi) &= L_1^{-1}(G_2(x, y) - R2 - \\ N_2), L_1^{-1}(L_1\theta) & \end{aligned}$$

$$\begin{aligned} \psi_1 &= yC_1 + y^3C_2 + C_3 + \frac{1}{80640\xi^9} y^5 \left(\frac{1}{\eta} 24\xi^2 (360qy^2\delta^2\eta\xi'^4 + 120y^2\delta^2\eta\xi\xi'^2 (2\xi'^2 - 3q\xi'')) + \right. \\ &12\xi^2 (-42q\delta^2\eta\xi'^4 + 3qy^2\delta^2\eta\xi''^2 + \xi'^2 (qy^2\delta^2 + 84q\eta - 24y^2\delta^2\eta\xi'')) + 4qy^2\delta^2\eta\xi'\xi^{(3)} + \\ &+ 21\xi^5 (4 + q\delta^2\xi'' + q\delta^2\eta\xi^{(4)}) - 2\xi^4 (-21q + 21q\delta^2\xi'^2 + 2(y^2\delta^2 + 84\eta)\xi'' + 63q\delta^2\eta\xi''^2 \\ &+ 84q\delta^2\eta\xi'\xi^{(3)} + 2y^2\delta^2\eta\xi^{(4)}) + 3\xi^3 (-q(y^2\delta^2 + 84\eta)\xi'' + 12y^2\delta^2\eta\xi''^2 + 4\xi'^2 (y^2\delta^2 + 84\eta \\ &+ 63q\delta^2\eta\xi'') + 16y^2\delta^2\eta\xi'\xi^{(3)} - qy^2\delta^2\eta\xi^{(4)} \left. \right), \end{aligned} \quad 23$$

$$= L_1^{-1}(G_3(x, y) - R3 - N_3), \quad 20$$

$$\text{Then } L_2^{-1}(L_2\psi) = \psi - \sum_{j=0}^3 \frac{y^j}{j!} a_j(x)$$

where $a_j(x)$ are the integration constants which can be calculated based on the specific condition, ϕ and θ are the same, consequently

$$\left. \begin{aligned} \psi(x, y) &= \sum_{j=0}^{4-1} \frac{y^j}{j!} a_j(x) + L_2^{-1}(G_1(x, y) - R1 - N_1) \\ \phi(x, y) &= \sum_{j=0}^{2-1} \frac{y^j}{j!} b_j(x) + L_1^{-1}(G_2(x, y) - R2 - N_2) \\ \theta(x, y) &= \sum_{j=0}^{2-1} \frac{y^j}{j!} c_j(x) + L_1^{-1}(G_3(x, y) - R3 - N_3) \end{aligned} \right\} \quad 21$$

The partial differential equations solution is given as Eq. 17, Where ψ_0 , ϕ_0 and θ_0 are the functions including the boundary condition, forcing function $G_i(x, y)$ and the integral constants, the other components can be obtained by the recursive relation, the nonlinear term N_i can be represented by the infinite series of Adomian polynomials A_m shown in the form

$$N_i = \sum_{m=0}^{\infty} A_m(\psi_0, \psi_1, \dots, \psi_m, \theta_0, \theta_1, \dots, \theta_m, \phi_0, \phi_1, \dots, \phi_m) \quad 22$$

Where A_m are the Adomian polynomials for the specific non-linearity, the Adomian polynomials A_m for nonlinear terms N_i can be computed by using the following expression:

$$A_m = \frac{1}{m!} \frac{d^m}{dj^m} \left(N_i \left(\sum_{i=0}^m J^i F_i \right) \right) \Big|_{J=0}, m \geq 0$$

Where F_i are nonlinear term components.

Method of the Solution:

Using the Adomian decomposing method to solve the nonlinear systems of Eqs 13, 14 and 15 with the corresponding boundary condition Eq 16, the result is as follows:

$$\psi_0 = \frac{y^3}{6} \left(-\frac{3(q+2\xi)}{2\xi^3} \right) + y \left(\frac{3q+2\xi}{4\xi} \right),$$

$$\phi_0 = -\frac{1}{2}ERmA_3\xi^2 + \frac{1}{2}ERmy^2A_3,$$

$$\phi_1 = C_4 + yC_5 - \frac{1}{20\xi^4}RmA_3\left(\frac{1}{6}ERmy^6\delta A_3(3q + 4\xi)\xi' - \frac{5}{4}y^4\xi(q + 2ERm\delta A_3\xi^2\xi' + 2\xi(1 + EqRm\delta A_3\xi'))\right) + \frac{5}{2}y^2\xi^3\left(3q + \xi(2 + 3EqRm\delta A_3\xi' - 4E\delta^2\xi'^2) + 2E\delta\xi^2(RmA_3\xi' - 2\delta\xi'')\right), \quad 24$$

$$\theta_0 = -y\left(\frac{1}{2\xi}\right) - \frac{y^2\beta}{2A_4} + \frac{A_4 + \beta\xi^2}{2A_4},$$

$$\theta_1 = C_6 + yC_7 + C_8 - \frac{1}{16A_4^5\xi^{10}}\left(\frac{2}{3}y^3A_4\xi^7(12Rd\beta A_4^2\xi^2 + 36Rd\beta^2A_4\xi^4 + 18Rd\beta^3\xi^6 - A_4^3(6Rd + Re\delta A_5p_r\xi\xi')) + 2\delta^2A_4^4(-2\xi'^2 + \xi\xi'')\right) - 2y^2\xi^8(3Rd\beta^2A_4^2\xi^4 + 6Rd\beta^3A_4\xi^6 + 2Rd\beta^4\xi^8 + \beta A_4^3\xi^2(-4Rd + Re\delta A_5p_r(3q + 2\xi)\xi') - A_4^4(3Rd + 4\beta\delta^2\xi^2\xi'^2 + 4\beta\delta^2\xi^3\xi''))), \quad 25$$

The constants coefficients $C_1, C_2, C_3, C_4, C_5, C_6, C_7$ and C_8 are large. Coefficients can be determined by using the boundary condition equation Eq. 16 and MATHEMATICA software. As a result, the approximate solution is to use the first ψ_0 and second ψ_1 .

$$\psi = \psi_0 + \psi_1 + \dots, \phi = \phi_0 + \phi_1 + \dots, \theta = \theta_0 + \theta_1 + \dots \quad 26$$

The gradient of magnetic pressure is obtained from Eq 26 to Eq 18, which yields

$$\frac{\partial P_m}{\partial x} = A_1Re\delta(\psi_y\psi_{xy} - \psi_x\psi_{yy}) + A_2\nabla^2\psi_y + S^2Re(\delta\phi_y\phi_{xy} - \delta\phi_x\phi_{yy} + \phi_{yy}) - \frac{A_2}{\eta}(\psi_x + 1),$$

$$\frac{\partial P_m}{\partial y} = A_1Re\delta^3(\psi_y\psi_{xx} - \psi_x\psi_{yy}) - A_2\delta^2\nabla^2\psi_x - S^2Re\delta^2(\delta\phi_y\phi_{xx} - \delta\phi_x\phi_{xy} + \phi_{xy}) + \frac{A_2}{\eta}\delta^2\psi_x, \quad 27$$

Results and Discussion

This part looks at the graphical results of a variety of important parameters used in the suggested modeling. The graphs Figs. 2-12 are specifically for streamlines, axial velocity, magnetic pressure, magnetic force, contours, temperature, Nusselt number and pressure gradient profile. To make it more meaningful, several cases were examined, including permeability parameters η , Hartmann number M , electric field parameter E , Reynolds number Re , and magnetic Reynolds number Rm . The numerical values were

And the magnetic pressure profile is obtained from Eq. 27 by being integral with y , which yields

$$P_m = \int_0^y A_1Re\delta^3(\psi_y\psi_{xx} - \psi_x\psi_{yy}) - A_2\delta^2\nabla^2\psi_x - S^2Re\delta^2(\delta\phi_y\phi_{xx} - \delta\phi_x\phi_{xy} + \phi_{xy}) + \frac{A_2}{\eta}\delta^2\psi_x dy, \quad 28$$

The distribution of the dimensionless shear stress has the following form:

$$\tau_{xy} = A_2(\psi_{yy} - \delta^2\psi_{xx}) \quad 29$$

also, the electric field E is obtained from

$$E = \psi_y - \delta(\psi_y\phi_x - \psi_x\phi_y) + \frac{1}{A_3R_m}\nabla^2\phi, \quad 30$$

The dimensionless form of the bulk mean temperature is shown by

$$\theta_m = \int_0^\xi \theta \psi_y dy / \int_0^\xi \psi_y dy, \quad 31$$

Moreover, the Nusselt number is represented as

$$Nu = -1/\theta_m A_4.$$

chosen based on the previous literature²⁷ and trapping for flow is discussed graphically. All figures are plotted using the Mathematica 12 program.

Axial Velocity Profile

The axial velocity mechanism is displayed in Fig 2 in relation to the physical parameters. The graphical results are shown in Fig 2. We can observe that the axial velocity u shows a dual mechanism. Fig 2a

shows the axial velocity decline for Cu nanofluid, base fluid (blood), hybrid nanofluid, and Au nanofluid. Its behavior is reversed on the other side. The effect of permeability of porous medium η on axial velocity u is investigated in Fig 2b, which shows that increasing the permeability η decreases the axial

velocity u . Fig 2c. illustrates that large values of the Hartmann number M tend to increase the axial velocity. The magnetic Reynolds number Rm is discussed in Fig 2d the axial velocity increases when the parameter Rm increases.

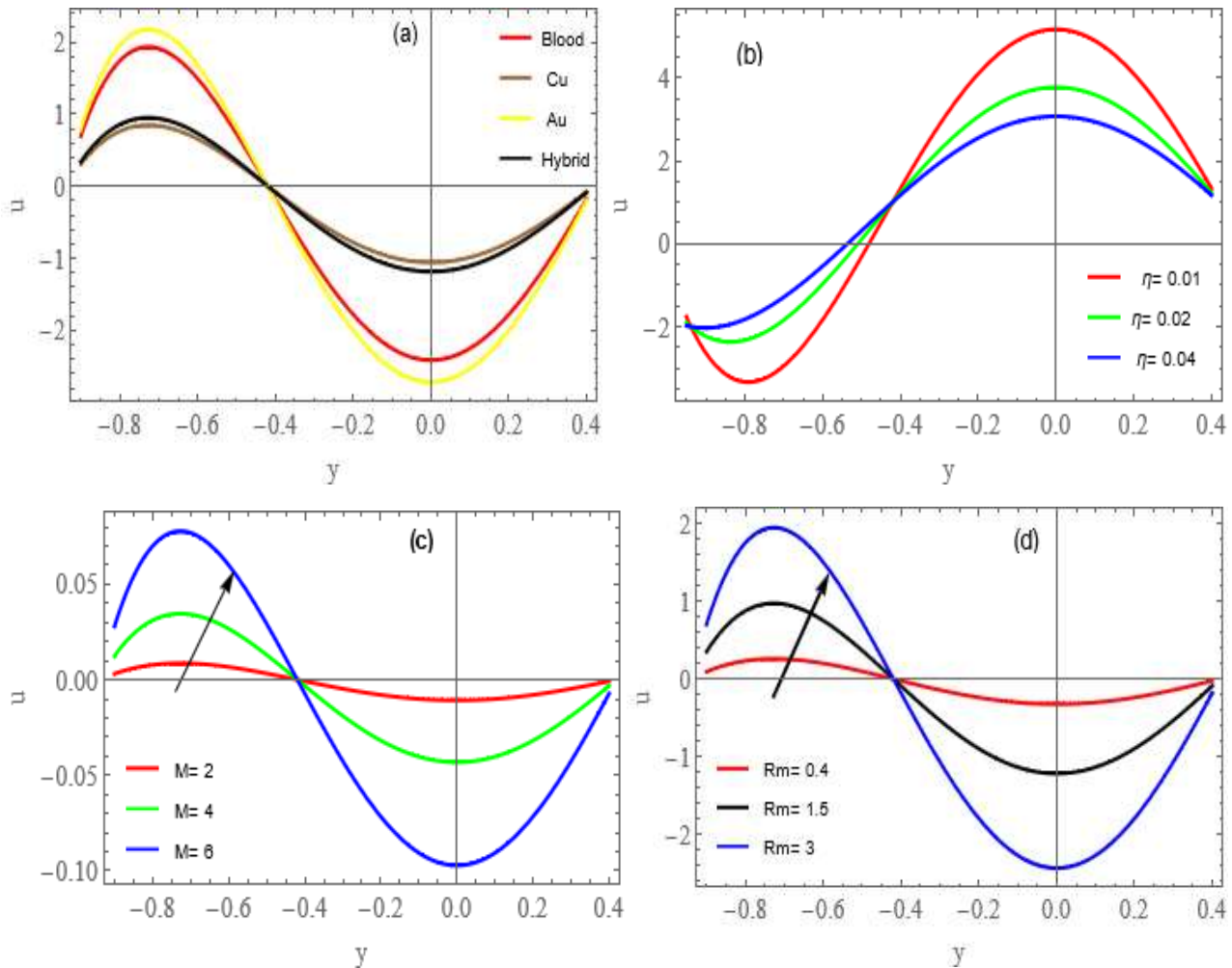


Figure 2. Axial velocity profiles for different fluid parameters

Temperature Profile:

The effect of physical parameters on the temperature profile θ is represented in Fig 3. Both Figs 3a, and 3b show that the effect of thermal radiation R_d and absorption parameters β on the temperature profile is improved by both parameters. As shown in Fig 3a, an increase in the radiation parameter led to an increase in the propagation of electromagnetic waves while decreasing heat conduction. It has a significant effect on thermal diffusion in a system later on. When it is extinguished, the nearby molecules move less

vigorously and transport less energy between them because heat transfer diffusion happens due to random molecular motion. The Eckert number E_c improves the temperature profile as shown in Fig 3c. The increased Eckert number E_c indicates that advective transport is important in improving the temperature profile. This finding is similar to that of Abo-Elkhair et al¹². Fig 3d shows that the Prandtl number firstly opposes the temperature profile. On the other hand, its behavior begins to change and becomes reverse.

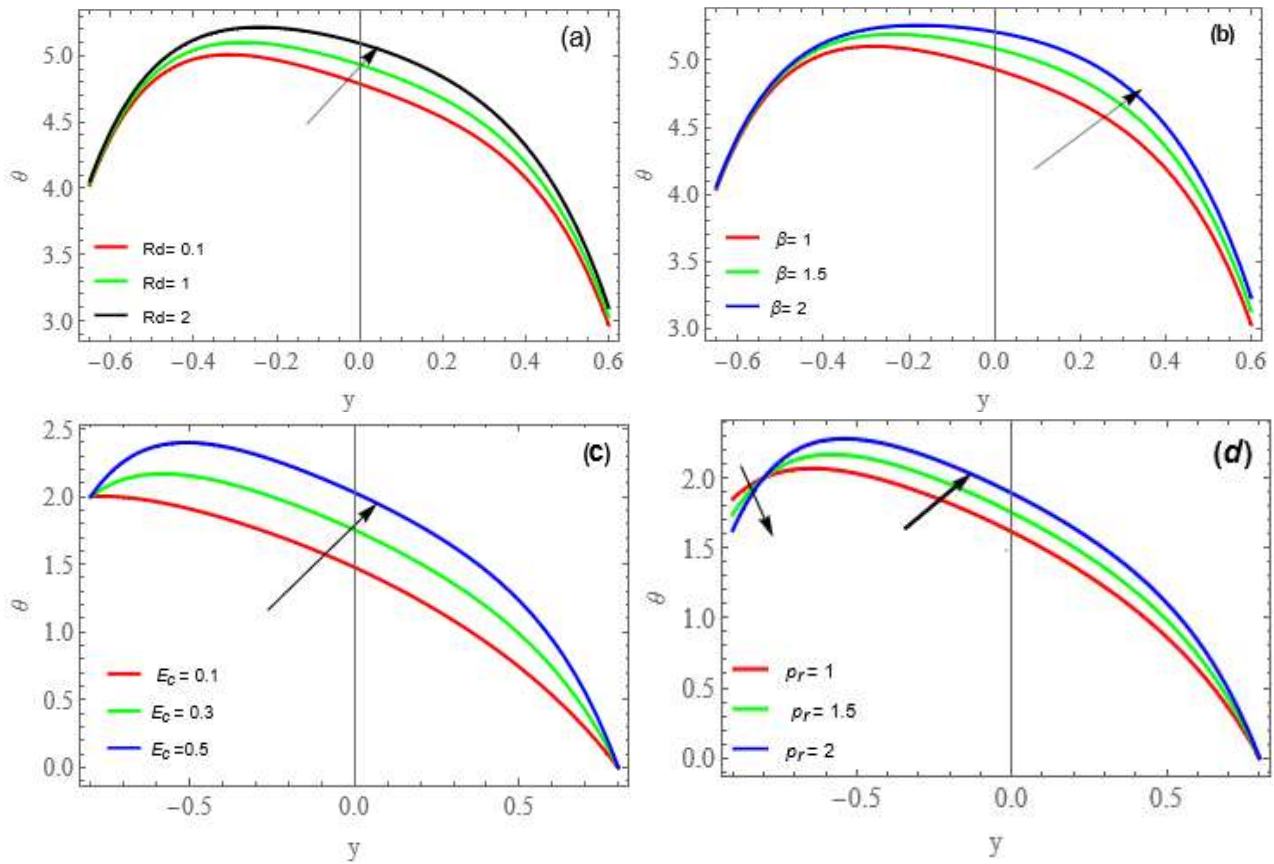


Figure 3. Temperature profiles for different fluid parameters.

Pressure Gradient Profile:

The influence of parameters that matter with respect to the pressure gradient can be shown graphically in Fig. 4. These graphs are plotted between $\partial p/\partial y$ vs X,Y.

Fig 4 shows that the pressure gradient is undulating along the Y-axis and X-axis, although it varies more rapidly along the y-axis. Observing in Figs 4a, and 4b, the pressure gradient has a double mechanism, it increases in the first half of ($y < 0$) due to an

increase in the parameters M and Rm but decreases in the other half ($y > 0$). Fig 4d and Fig 4e show the reverse conduct for the pressure gradient along x-axis, which means that the pressure gradient is diminishing along the channel as M and Rm values increase. The Reynolds number Re increase in the first half ($y < 0$) for increasing values, but it begins to change its situation and behavior in the next half ($y > 0$) as shown in Fig 4c The pressure gradient along the x-axis decreases remarkably, so Reynolds number Re rises through Fig 4f.

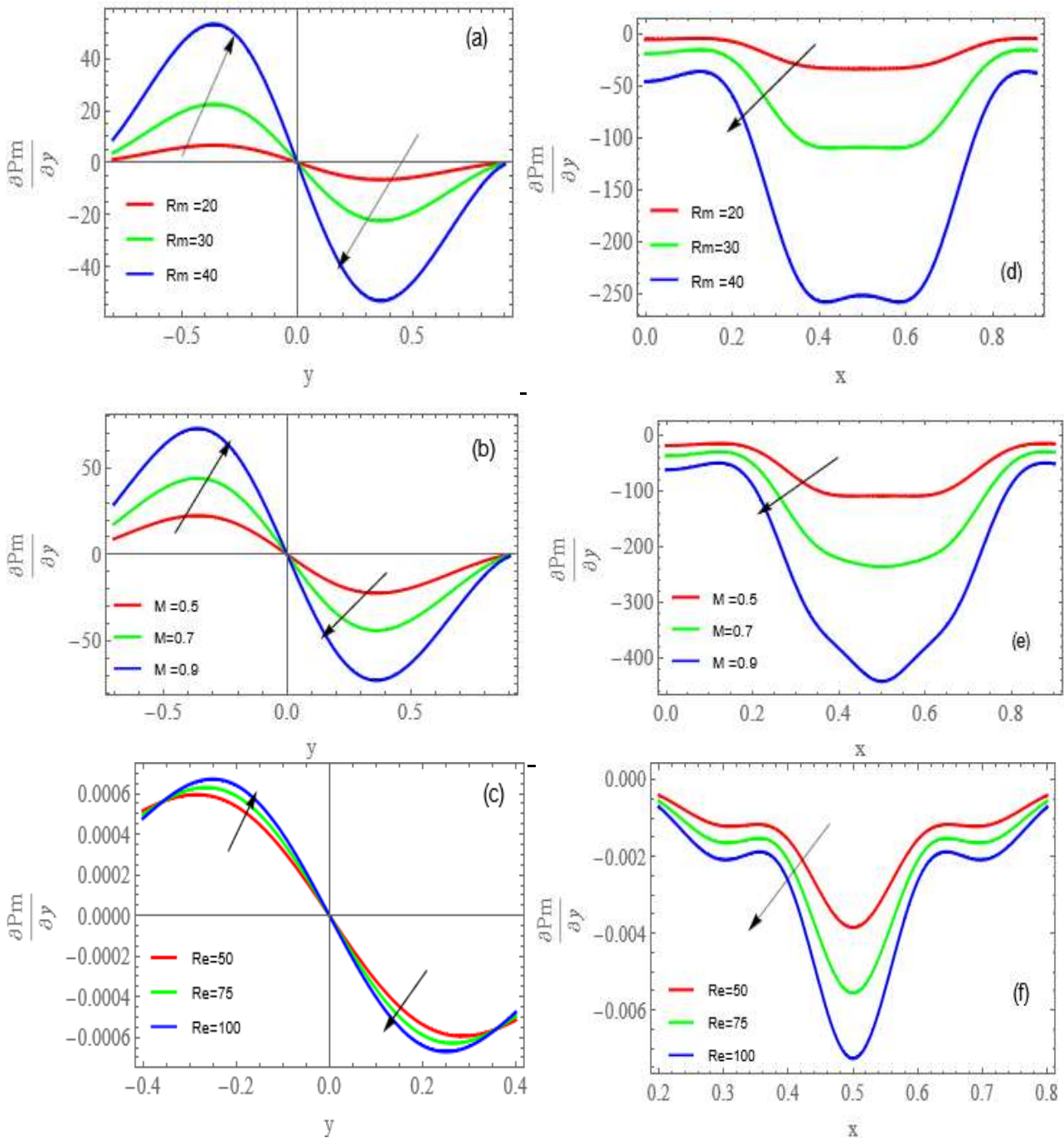


Figure 4. Pressure gradient profiles for different fluid parameters.

Magnetic Pressure Profile:

The graphical results for the magnetic pressure profile P_m are illustrated in Fig 5.

The effect of the magnetic Reynolds number R_m and Hartmann number M on the magnetic pressure is shown in Figs 5a, and 5b. When the values of R_m and M increase, the magnetic pressure P_m decreases along the entire channel. The influence of the

permeability of porous medium η on the magnetic pressure profile in the peristaltic pumping region is seen in Fig 5c. It was observed that the parameter η leads to decrease in magnetic pressure to begin with, but soon the reverse occurs, causing the profile of magnetic pressure to progressively increase with height and in the range. In Fig 5d is depicted the impact of Reynolds number Re on the

magnetic pressure profile P_m . The magnetic

pressure P_m opposes Re increase.

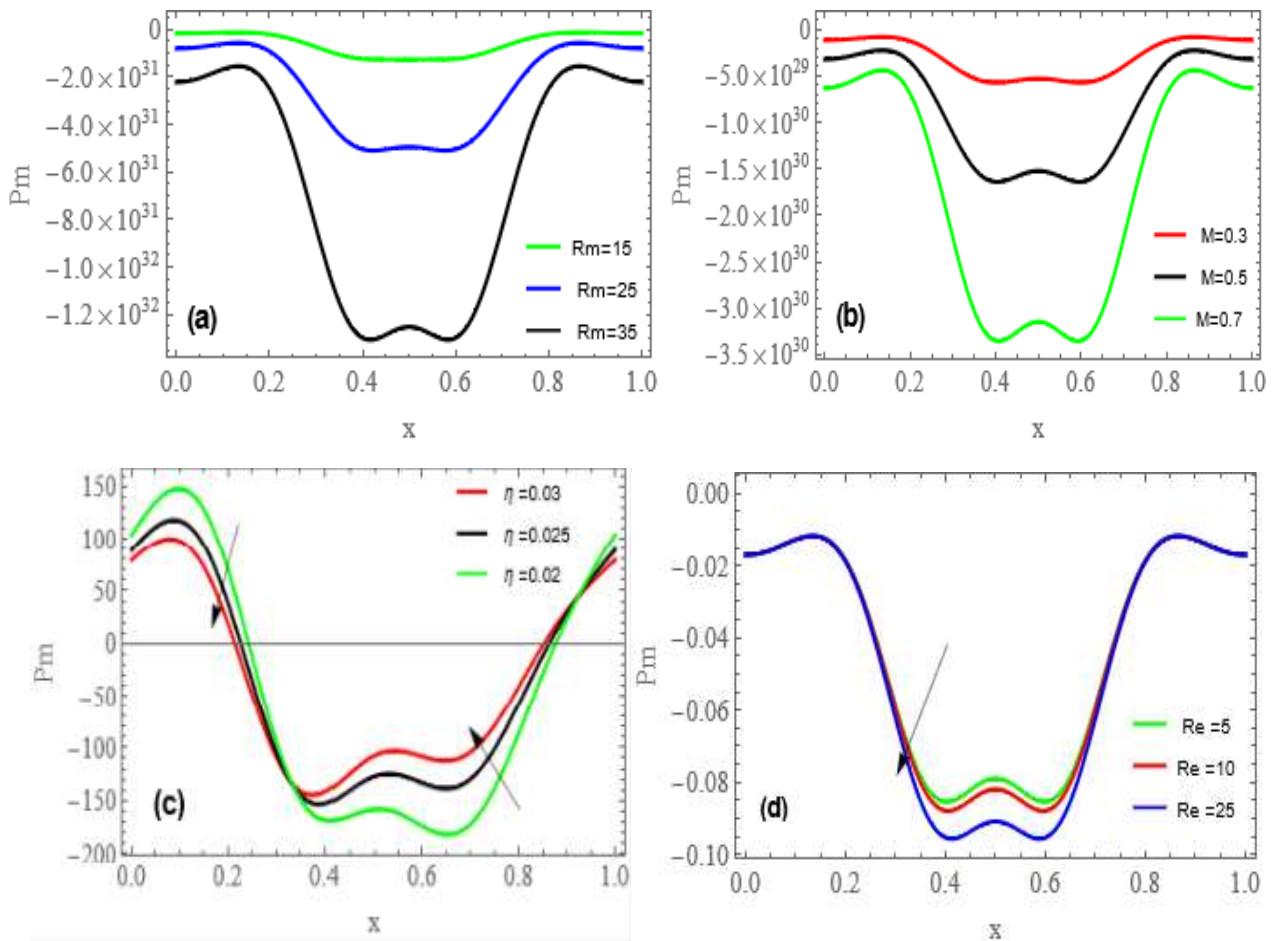


Figure 5. Magnetic pressure profiles for different fluid parameters.

Nusselt Number Profile:-

The Nusselt number Nu is utilized to determine the heat transfer between a solid body and a moving fluid. Figure 6 displays the plots of the Nusselt number Nu versus the wavenumber δ . The Nusselt number profile for the hybrid nanofluid in Fig 6a, is higher than that of the gold and copper nanofluids, as well as it higher than that of the base fluid (blood). Fig 6b shows a view on the permeability of porous media η on the Nusselt number profile Nu and it found that Nu

diminishes with an increase in the permeability parameter η . The result of the heat absorption parameters β on the Nusselt number profile Nu is shown in Fig 6c. This indicate that the performance of β on Nusselt number profile is quite opposite as compared to those of permeability parameters η . Fig 6d indicates that as the magnetic Reynolds number Rm increases, the Nusslet number profile Nu decreases.

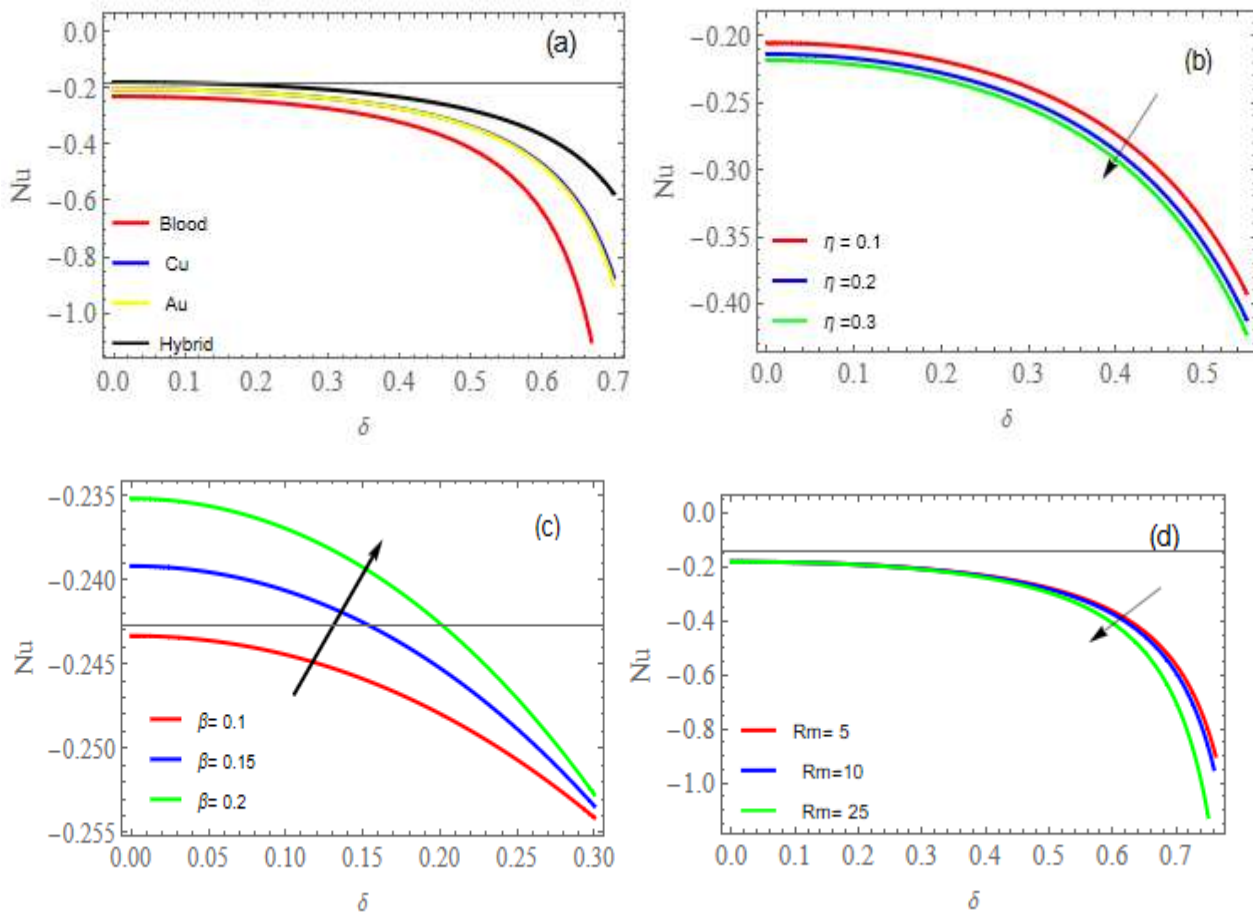


Figure 6. Nusselt number profiles for different fluid parameters.

Trapping Phenomenon:

The trapping mechanism refers to the creation of a bolus of fluid through enclosed streamlines. Because the entrapped bolus is surrounded by a peristaltic wave, it flows at the same speed as the wave. This mechanism has important significance in physiology according to fluid flow mechanics. This mechanics implies complexity, which is useful for investigating peristaltic flows. Fig 7 illustrates the conduct of Hartmann number M to the trapping mechanism, as can be seen in these diagrams as the M rises, the trapping bolus reduces while the number of bolus rises slowly. Fig 8 shows that the permeability parameters η reduce the number of trapped boluses when permeability parameter η values are

increasing. The trapped bolus's size is increasing as the magnetic Reynolds number Rm rises, as shown in Fig 9.

Figs 10–12 show the development of magnetic force contours to define the presence of physical parameters. As can be seen in Fig 10, magnetic force contours run in the same direction. The wave amplitude ϵ raises the magnetic force contours greatly because of the increase in the wave amplitude magnitude as the flow field. As shown in Fig 11, the magnetic force contours decrease as the value of the electrical field E increases. It is clear that in Fig 12, when the magnetic Reynolds number Rm rises, the magnetic force contours shrink while the number of lines increases gradually.

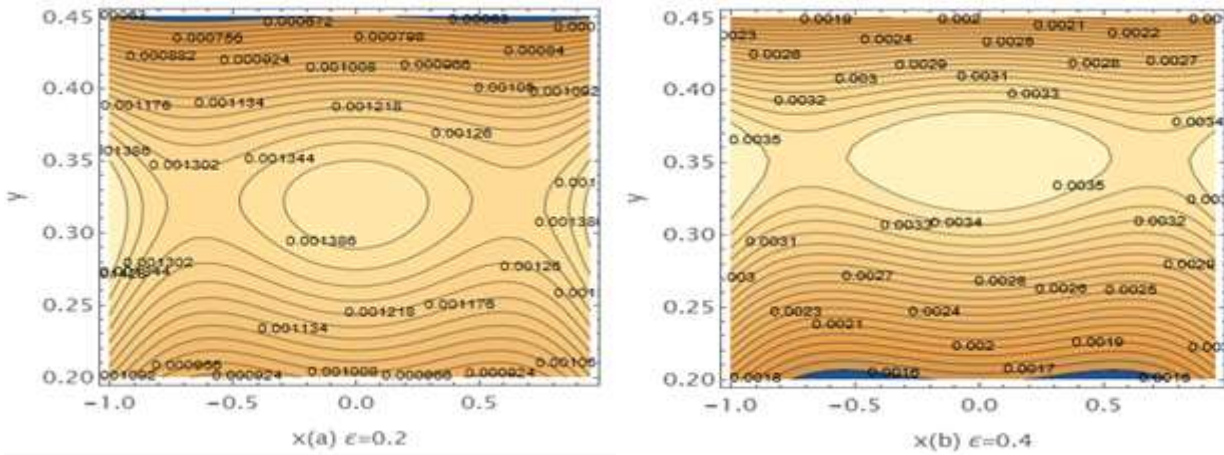


Figure 10. Impact of wave amplitude ϵ on the magnetic force contours

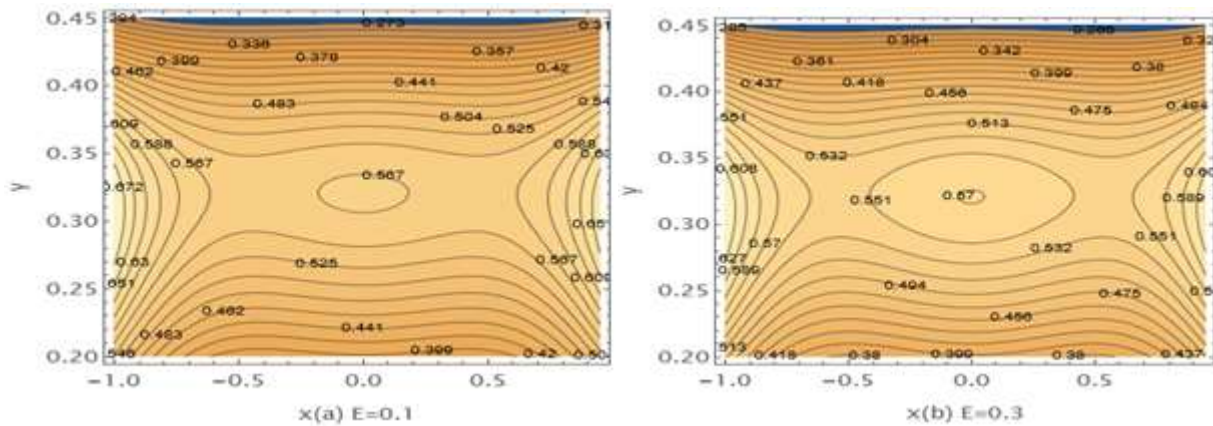


Figure 11. Impact of electrical field E on the magnetic force contours

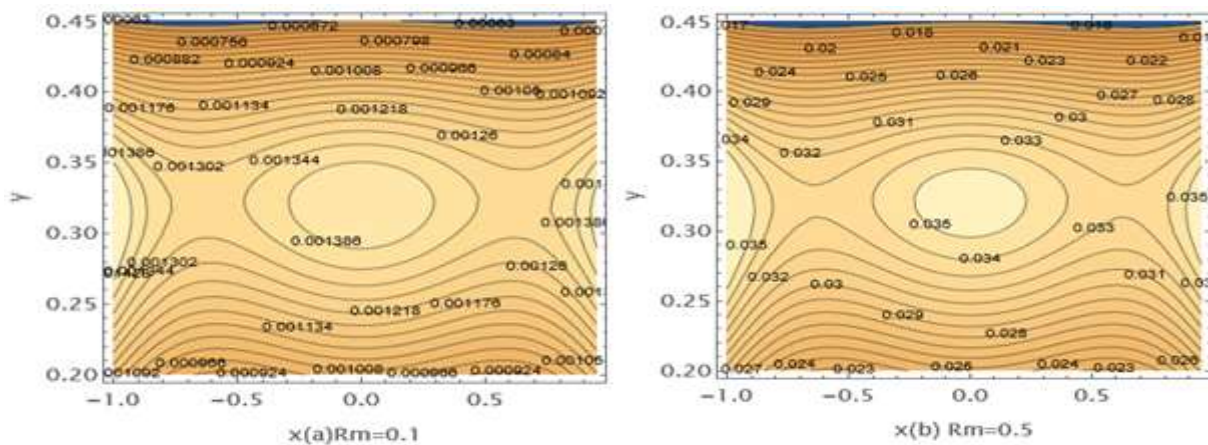


Figure 12. Impact of Rm on the magnetic force contours

Conclusion

The effect of nonlinear thermal radiation and magnetic force on the peristaltic transport of hybrid bio-nanofluid with a porous medium in a symmetric channel under the influence of magnetic fields with

high and low Reynolds numbers has been investigated. Blood is considered base fluid which is non-Newtonian and Cu-Au as nanoparticles. Momentum, Maxwell, and heat are studied in the

dimensionless form as a system of nonlinear partial differential equations with nonlinear thermal radiation equations. Graphical results are presented for the axial velocity, temperature, pressure gradient, Nusselt number, magnetic pressure, magnetic force contours, and trapping, the major findings of this study are outlined as follows:

- The axial velocity u curves and pressure gradient along y exhibit dual mechanisms.
- The gold nanoparticle has a higher velocity as compared to the base fluid (blood), hybrid nanoparticles, and copper nanoparticles
- The magnetic field and magnetic Reynolds number improved the axial velocity.
- The radiation parameters, Eckert number, and heat absorption parameters improved the temperature profile.
- For Reynolds number Re , the influence of the pressure gradient along the x direction decreases dramatically.
- The magnetic pressure profile decreases with increasing magnetic Reynolds number

R_m , Reynolds number, and magnetic field M , however, the permeability of the porous medium improves magnetic pressure.

- For the heat absorption parameter, the rate of heat transfer (Nusselt number) increases while the permeability of the porous medium and the magnetic Reynolds number decrease.
- For hybrid nanofluids, followed by gold, copper, and base fluid, the rate of heat transfer (Nusselt number) displays a rising tendency.
- Hartmann number and magnetic Reynolds number significantly increase the size of trapping boluses, whereas permeability parameters reduce trapping boluses in generating.

These results might have an impact on MRI blood flow imaging in people, particularly if gold, copper, or both nanoparticles are used to treat cancer and tumors.

Authors' Declaration

- Conflicts of Interest: None.
- We hereby confirm that all the Figures and Tables in the manuscript are ours. Furthermore, any Figures and images, that are not ours, have been included with the necessary permission for

re-publication, which is attached to the manuscript.

- Ethical Clearance: The project was approved by the local ethical committee in University of Baghdad.

Authors' Contribution Statement

The research's fundamental idea was offered by A. M. A., and it was then mathematically applied by A. M. N. using the Mathematica program. Both

researchers gave an overview of their work as well as the main findings.

References

1. Latham TW. Fluid motions in a peristaltic pump: Massachusetts Institute of Technology, Cambridge. MSc Thesis; 1966.
2. Shapiro AH, Jaffrin MY, Weinberg SL. Peristaltic pumping with long wavelengths at low Reynolds number. *J Fluid Mech.* 1969; 37(4): 799-825. <https://dx.doi.org/10.1017/S0022112069000899>
3. Chen PC, Mwakwari SC, Oyelere AK. Gold nanoparticles: from nanomedicine to nanosensing. *Nanotechnol Sci Appl.* 2008; 1: 45- 65. <https://dx.doi.org/10.2147/NSA.S3707>
4. Cardinal J, Klune JR, Chory E, Jeyabalan G, et al. Noninvasive radiofrequency ablation of cancer targeted by gold nanoparticles. *Surgery.* 2008; 144(2): 125-132. <https://dx.doi.org/10.1016/j.surg.2008.03.036>
5. Gawande MB, Goswami A, Felpin F-X, Asefa T, Huang X, Silva R, et al. Cu and Cu-based nanoparticles: synthesis and applications in catalysis. *Chem Rev.* 2016; 116(6): 3722-3811. <https://dx.doi.org/10.1021/acs.chemrev.5b00482>
6. Zhang L, Bhatti MM, Marin M, S. Mekheimer K. Entropy analysis on the blood flow through



- anisotropically tapered arteries filled with magnetic zinc-oxide (ZnO) nanoparticles. *Entropy*. 2020; 22(10): 1070. <https://dx.doi.org/10.3390/e22101070>
7. Tripathi D, Prakash J, Gnanaswara Reddy M, Kumar R. Numerical study of electroosmosis-induced alterations in peristaltic pumping of couple stress hybrid nanofluids through microchannel. *Ind. J Phys.* 2021; 95(11): 2411-2421. <https://dx.doi.org/10.1007/s12648-020-01906-0>
 8. Mishra S, Pattnaik P, Baag S, Bhatti M. Study of Kerosene–Gold–DNA Nanoparticles in a Magnetized Radiative Poiseuille Flow with Thermo-Diffusion Impact. *J Comput Biophys Chem.* 2022: 1-12. <https://dx.doi.org/10.1142/S2737416523400045>
 9. Hussain F, Nazeer M, Altanji M, Saleem A, Ghafar M. Thermal analysis of Casson rheological fluid with gold nanoparticles under the impact of gravitational and magnetic forces. *Case Stud. Therm Eng.* 2021; 28: 101433. <https://dx.doi.org/10.1016/j.csite.2021.101433>
 10. Noreen S, Rashidi M, Qasim M. Blood flow analysis with considering nanofluid effects in vertical channel. *Appl Nanosci.* 2017; 7(5): 193-199. <https://dx.doi.org/10.1007/s13204-017-0564-0>
 11. Rashid M, Ansar K, Nadeem S. Effects of induced magnetic field for peristaltic flow of Williamson fluid in a curved channel. *Physica A.* 2020; 553: 123979. <https://dx.doi.org/10.1016/j.physa.2019.123979>
 12. Abo-Elkhair R, Bhatti M, Mekheimer KS. Magnetic force effects on peristaltic transport of hybrid bio-nanofluid (AuCu nanoparticles) with moderate Reynolds number: An expanding horizon. *Int. Commun. Heat Mass Transf.* 2021; 123: 105228. <https://dx.doi.org/10.1016/j.icheatmasstransfer.2021.105228>
 13. Murad MA, Abdulhadi AM. Influence of heat and mass transfer on peristaltic transport of viscoplastic fluid in presence of magnetic field through symmetric channel with porous medium. *J Phys Conf Ser;* 2021; 1804(1):012060. <https://dx.doi.org/10.1088/1742-6596/1804/1/012060>
 14. Khudair WS, Dwail HH. Studying the Magnetohydrodynamics for Williamson Fluid with Varying Temperature and Concentration in an Inclined Channel with Variable Viscosity. *Baghdad Sci J.* 2021; 18(3): 0531-0538. <https://dx.doi.org/10.21123/bsj.2021.18.3.0531>
 15. Al-Khafajy DGS. Influence of Varying Temperature and Concentration on Magnetohydrodynamics Peristaltic Transport for Jeffrey Fluid with a Nanoparticles Phenomenon through a Rectangular Porous Duct. *Baghdad Sci J.* 2021; 18(2): 279-295. <https://dx.doi.org/10.21123/bsj.2021.18.2.0279>
 16. Kareem RS, Abdulhadi AM. Impacts of Heat and Mass Transfer on Magneto Hydrodynamic Peristaltic Flow Having Temperature-dependent Properties in an Inclined Channel Through Porous Media. *Iraq J Sci.* 2020; 61(4): 854-869. <https://dx.doi.org/10.24996/ijis.2020.61.4.19>
 17. Ahmed B, Hayat T, Alsaedi A. Mixed convection peristalsis of hybrid nanomaterial flow in thermally active symmetric channel. *Case Stud Therm Eng.* 2021; 27: 101272. <https://dx.doi.org/10.1016/j.csite.2021.101272>
 18. Musawi BA, Abdulhadi AM. Influence of heat transfer analysis and (MHD) on peristaltic transport of ree-eyring fluid in rotating frame. *AIP Conf Proc.* 2023; 2414(1): 040076. <https://dx.doi.org/10.1063/5.0116630>
 19. Jawad QK, Abdulhadi AM. Influence of MHD and Porous Media on Peristaltic Transport for Nanofluids in An Asymmetric Channel. *Iraq J Sci.* 2023; 64(3):1344-1360 <https://dx.doi.org/10.24996/ijis.2023.64.3.28>
 20. Akram J, Akbar NS, Tripathi D. Blood-based graphene oxide nanofluid flow through capillary in the presence of electromagnetic fields: A Sutterby fluid model. *Microvasc.Res.* 2020; 132: 104062. <https://dx.doi.org/10.1016/j.mvr.2022.104435>
 21. Tripathi D, Prakash J, Tiwari AK, Ellahi R. Thermal, microrotation, electromagnetic field and nanoparticle shape effects on Cu-CuO/blood flow in microvascular vessels. *Microvasc Res.* 2020; 132: 104065. <https://dx.doi.org/10.1016/j.mvr.2020.104065>
 22. Bhatti MM, Marin M, Zeeshan A, Abdelsalam SI. Recent trends in computational fluid dynamics. *Front Phys.* 2020; 8: 593111. <https://dx.doi.org/10.3389/fphy.2020.593111>
 23. Kareem Z, Tawfiq L. Recent Modification of Decomposition Method for Solving Nonlinear Partial Differential Equations. *J Adv Math.* 2020;18:154-161. <https://dx.doi.org/10.24297/jam.v18i.8744>
 24. Mjithap HZ, Al-Azzawi SN. Mixing Sumudu transform and Adomain decomposition method for solving Riccati equation of variable fractional order. *J Interdiscip Math.* 2019;22(8):1559-1563 <https://dx.doi.org/10.1080/09720502.2019.1706858>.
 25. Shit G, Ranjit N, Sinha A. Adomian decomposition method for magnetohydrodynamic flow of blood induced by peristaltic waves. *J Mech Med Biol.* 2017; 17(01): 1750007. <https://dx.doi.org/10.1142/S0219519417500075>
 26. Bakodah HO, Ebaid A. The Adomian decomposition method for the slip flow and heat transfer of nanofluids over a stretching/shrinking sheet. *Rom Rep Phys.* 2018; 70: 115.
 27. Raza M, Ellahi R, Sait SM, Sarafraz M, Shadloo MS, Waheed I. Enhancement of heat transfer in peristaltic flow in a permeable channel under induced magnetic field using different CNTs. *J Therm Anal Calorim.* 2020; 140(3): 1277-1291. <https://dx.doi.org/10.1007/s10973-019-09097-5>

النقل التمعجي لمائع لانيوتيني تحت تأثير القوة المغناطيسية وانتقال الحرارة في قناة متمائلة عبر وسط مسامي

امال محي نصيف، احمد مولود عبد الهادي

قسم الرياضيات، كلية العلوم، جامعة بغداد، بغداد، العراق.

الخلاصة

في هذا البحث تم مناقشة تأثير القوة المغناطيسية والاشعاع الحراري للنقل التمعجي للسائل النانوي الهجين عبر وسط مسامي في قناة متناظرة. تم استخدام طريقة (Adomain decomposition) لتوضيح السرعة المحورية، دالة الجريان، درجة الحرارة، تدرج الضغط، ضغط المغناطيسي وقوة المغناطيسية. تظهر النتائج ان جسيمات الذهب النانوية لها سرعة ارتفاع مقارنة بجسيمات النحاس النانوية والسائل النانوي الهجين، والقوة المغناطيسية تزداد عندما يزداد اتساع الموجة. تم فحص درجة الحرارة ومعدل نقل الحرارة بوضوح، ولقد لوحظ أن ارتفاع الإشعاع الحراري يزيد من درجات الحرارة. اخيرا، تم عرض ظاهرة التكوين لشرح سلوك الفيزيائي للمعلمات، تم رسم تأثير المعلمات الفيزيائية باستخدام برنامج الـ MATHEMATICA.

الكلمات المفتاحية: قوة المغناطيسية، النقل التمعجي، الوسط المسامي، قناة متمائلة، الاشعاع الحراري.